Full length article

Switchable formation of diverse regular nanostructures on metal by dual correlated femtosecond laser irradiations

Bo Zhao [a,b], Xiaofang Zhou [a], Xin Zheng [c], Ruiping Wang [e], Yucai Lin [c], Tingting Zou [c], Zhenfen Huang [a], Changming Huang [a], Jianjun Yang [c,d,*]

[a] *Laboratory of Optical Field Manipulations, Department of Physics, Changzhi University, Changzhi, Shanxi 046011, China*
[b] *Advanced Ultraviolet Optoelectronics, Co., Ltd, Changzhi, Shanxi 046000, China*
[c] *GPL Photonics Laboratory, State Key Laboratory of Luminescence and Applications, Changchun Institute of Optics, Fine Mechanics and Physics, Chinese Academy of Sciences, Changchun 130033, China*
[d] *Center of Materials Science and Optoelectronics Engineering, University of Chinese Academy of Sciences, Beijing 100049, China*
[e] *Avic Changcheng Institute of Metrology & Measurement, Beijing 100095, China*

ARTICLE INFO

ABSTRACT

Manipulation of material properties via femtosecond laser-induced periodic surface structures is of significant importance for many practical applications in optics, tribology and wettability, but it is still a substantial challenge for single-beam femtosecond laser irradiation. We here report a strategy to uniformly generate large-area periodic nanostructures on molybdenum surface by utilizing cylindrical focusing of double time-delayed femtosecond blue lasers with orthogonal linear polarizations. It is found that three different types of periodic surface structures can be controlled and actively transformed through properly adjusting the energy fluence ratios between double laser pulses. The remarkable long-range uniform property is clearly identified by both the microscopic observation and Fourier frequency analysis. The obtained minimum structural size and period approximate 140 nm and 260 nm, respectively. The underlying mechanisms are attributed to the complex surface plasmon excitation during the temporally correlated dynamic process of dual laser-material interactions. These investigations help to facilitate femtosecond laser nanostructuring into a robust and versatile way.

1. Introduction

Recent research advances in femtosecond laser-induced periodic surface structures (fs-LIPSS), a universal phenomenon of the laser-matter interaction with the energy fluence near the damage threshold, open up a new avenue for controllable surface nanostructuring on diverse materials [1–5]. With the help of this maskless technology, different LIPSSs even with the nanoscale period can be manufactured over a large area for the proper laser parameters, which clearly demonstrates advantages over the conventional lithography methods often suffering complex procedures and low throughput [6–7]. The capability of fs-LIPSS in manipulating the essential surface properties of materials allows practical applications in optics, tribology, wettability, biomedicine, and etc [8–12]. The corresponding physical origins are still on debate with two theories: (i) surface electromagnetic interference making the spatially periodic deposition of the laser energy during the

laser-matter interaction; (ii) self-organization from the hydrodynamic motions of the surface melting layer [13]. To be sure, the formation of fs-LIPSS often undergoes a series of ultrafast dynamic processes in the time domain [14–16]. Now we can suppose that if more laser pulses are incident during the transient non-equilibrium stage of materials, the energy relaxation processes within the materials are modulated in both the temporal and spatial domains, which is expected to provide new opportunities for controlling the morphology of fs-LIPSSs.

Currently, the development of fs-LIPSS technology especially with single-beam femtosecond laser irradiation suffers two obstacles, i.e, irregular arrangement of the structures, and lacking diversity of the morphology, which present great challenges in the scope of surface functionalizations on multidisciplinary applications. In recent previous studies, temporally shaped femtosecond lasers have been tried to solve the aforementioned problems via exploiting the transient surface dynamics of the laser-material interaction [17–27]. For instance, through

using double/three/multiple femtosecond laser pulses with orthogonal/ cross/parallel polarizations and inter-pulse picosecond time delays, our group and Giannuzzi et al successfully manufactured the homogeneous large-area one-dimensional (1D) nanograting structures were on both metals and semiconductors [17–19], which overcomes the undesirable phenomena of bending, splitting and interruption. Moreover, with properly choosing the inter-pulse delay, energy fluence and polarization state of double femtosecond laser irradiations, diverse types of the regular two dimensional (2D) LIPSSs have been reported to achieve, such as square array of dots, hexagonal array of triangles and holes, chains of spindles [20–27]. During these investigations, the temporally delayed femtosecond laser pulses irradiation present the merits of more degrees of freedom for controlling the LIPSSs, but their high efficient manufacturing with high precision and uniformity as well as the profile transitions have been less explored.

In this paper, we present an effective strategy for controllable manufacturing of different nanoscale LIPSSs with large-area uniformity on molybdenum surface, through using cylindrical focusing of double femtosecond blue laser pulses having orthogonal polarizations and a ps time delay. When the energy fluence ratios between double laser pulses are varied, three types of periodic surface structures, i.e., 1D nanograting, 2D nanotriangle and nanodot structure arrays, can be developed especially with large-area homogeneity. The feature size and the spatial period of the achieved surface structures can be decreased down to 140 nm and 260 nm, respectively. The uniform distribution in a long range is detailedly analyzed in both the spatial and frequency domains. Moreover, the formation conditions of such regular surface structures are experimentally obtained for the effective transitions in terms of the total energy fluence and the double laser fluence ratio. Finally, the deep insights into their physical origins are provided in the frame of multiple surface plasmon excitations due to the transient correlation between dual laser-material interaction dynamics.

2. Experiments

Fig. 1 schematically depicts a strategy of periodic nanostructuring on metal surface upon irradiation of double time-delayed femtosecond laser pulses. Here, a commercial Ti:sapphire femtosecond laser amplifier (Spitfire Ace, Spectra Physics) was employed as a light source to deliver linearly polarized infrared ($\lambda = 800$ nm) pulse trains at the repetition rate of 1 kHz, leading to a large time interval of 1 ms between the two adjacent pulses. The measured pulse time duration of the laser is 40 fs. In terms of developing nanoscale LIPSS period, the infrared femtosecond laser was frequency-doubled into the blue light at $\lambda = 400$ nm via a beta-barium-borate (BBO) crystal, after which a spectral band-pass filter was placed for eliminating the fundamental light components. To achieve the inter-pulse time delay in picosecond scale, the blue laser was allowed to pass through a birefringent crystal of Yttrium vanadate (YVO$_4$), which results in splitting of each laser pulse into double sub-ones with orthogonal linear polarization but in a collinear propagation. For the 1.6-mm thick birefringent crystal, the available time delay between double pulses is of $\Delta t = 1.5$ ps [28]. Through rotating an azimuth angle (α) of the crystal relative to the direction of the incident blue laser polarization, we can continuously change the energy ratio between double pulses. Afterwards, such double femtosecond lasers were then focused by a cylindrical lens (with a focal length $f = 50$ mm) into a line-shaped beam spot due to the actual spatial confinement only happening in one-dimension. Under such circumstances, the resultant large focal spot can help to decline the severe intensity variation and improve the structuring efficiency as well, in contrast to the traditional tight focusing effect with a spherical optical lens. The whole energy of the double laser pulses was finely adjusted by a combination of a half-wave plate with a Glan-Taylor prism that was placed before the BBO crystal.

In the experiment, a 1 mm-thick Mo plate (with a purity > 99.8%) was selected as the sample material, because of its having the good thermal transfer and conductivity properties for many practical applications in microelectronics, space optics and fusion reactors [29–31]. To avoid the disturbing effect of the laser-induced air ionization, the sample surface was placed 250 μm away before the focus. The resultant laser intensity distribution on the sample surface was monitored by a Win-CamD (LCM, DataRay), which presents a line-shaped profile with a narrowly confined width of approximately 35 μm and an unaffected length of approximately 6 mm at $1/e^2$ of the peak intensity, respectively, as shown in Fig. 1(b). Under the fixed irradiation of double femtosecond
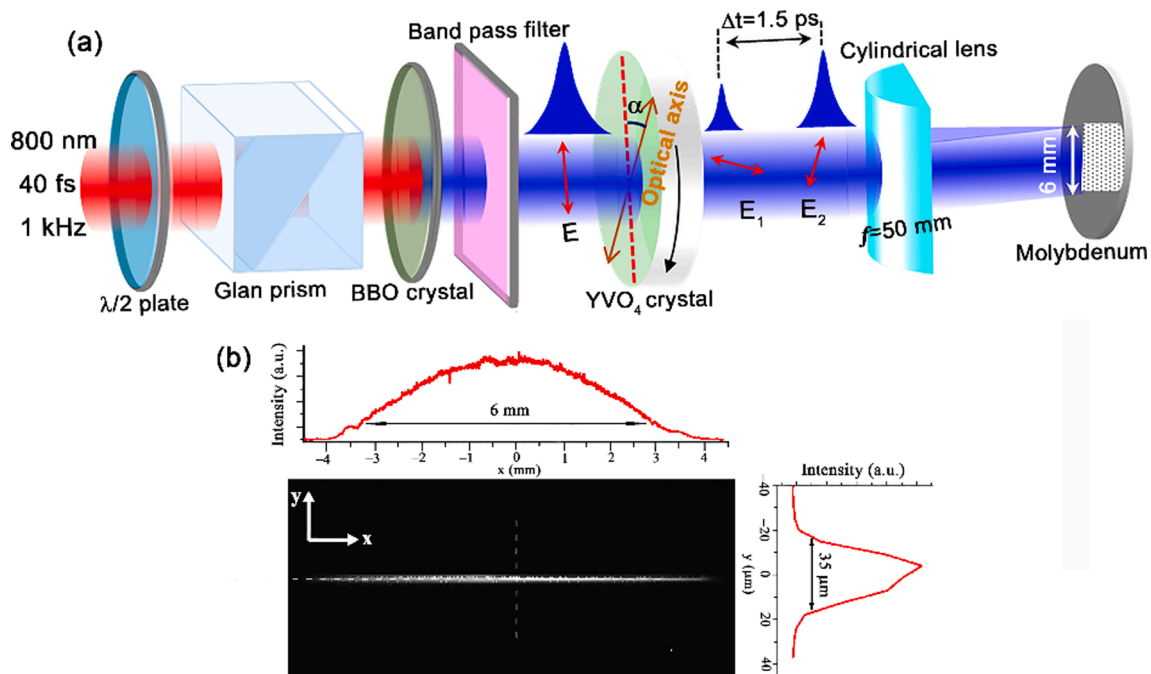

Fig. 1. (a) Schematic of the experimental setup for switchable formation of uniform large-area nanostructures on metal surface, by using double time-delayed femtosecond blue laser pulses with orthogonal linear polarizations (marked by E$_1$ and E$_2$, respectively) that are generated via a birefringent crystal of YVO$_4$. (b) Measured cylindrical focusing line-shaped beam spot on the sample surface and its cross-section profiles along two directions.

blue laser pulses, the mechanically polished Mo sample was mounted on a computer controlled X-Y-Z stage (XMS-100, Newport) to translate at a velocity of v = 0.01 mm/s along the confined direction of the line-shaped laser spot, resulting in about 3500 pulses partially overlapped within one laser spot area and a mm-scaled laser processing area in one-step. The laser peak energy fluence on the sample surface can be evaluated by $F = 8E_0/(\pi\phi_1\phi_2)$ [13], where E_0 represents the pulse energy, ϕ_1 and ϕ_2 for the confined and unconfined beam dimensions, respectively. Before and after the experiments, the sample material was ultrasonically cleaned in acetone solution for several hours, and the surface morphologies were characterized by a scanning electron microscope (FESEM, HITACI, S-4800).

The ablation threshold of the material is a vital parameter for the LIPSS formation. The reported ablation threshold fluence of Mo material was variable with laser parameters such as the laser wavelength, the overlapping pulse number and the pulse duration [32–33]. In the experiments, with the cylindrically focused double-beam laser scanning Mo surface at the velocity of $v = 0.01$ mm/s, the ablation threshold fluence was measured about $F_{th} = 0.057 \sim 0.071$ J/cm^2, depending on the energy fluence ratio between the double laser pulses.

3. Results and discussion

Before our experiments, various types of LIPSSs had been reported to develop on Mo surface in the previous literatures [20,34–38], as summarized in Table 1. Under the single-beam femtosecond laser irradiation with the linear polarization, 1D grating-like LIPSS was generally produced with orientation perpendicular to the laser polarization. The spatial period can be changed from the near- to deeply sub-wavelength scales by changing laser processing parameters [34–36]. Occasionally, 2D sporadic triangular and rhombic LIPSSs were observed to produce among the traditionally longitudinal LIPSS on local regions and vary dramatically in different regions [37]. Upon sequential scanning with two orthogonal laser polarization directions, 2D square-shaped nanopillars structure was also found to be achieved [36]. However, all LIPSSs above produced by the single-beam of femtosecond laser present irregular spatial distributions with undesirable bending, splitting and interruption defects. It was found that highly uniform 1D LIPSS can be achievable on thin Mo film [36]. Through using two-colored time-delayed femtosecond lasers, we successfully produced 2D nanodot-matrix LIPSS on bulk Mo [20]. In this work, we will employ double time-delayed blue femtosecond lasers to fabricate homogeneous large-area of three types of surface structures on the bulk Mo.

3.1. Structural morphology and characterization

In the experiment, by varying the azimuth angle of the birefringent crystal, α, we investigated the morphology evolution of the laser-induced surface structures on Mo surface with different energy ratios between double pulses at the total laser fluence of F = 0.182 J/cm^2. In the case of α = 0°, the double time-delayed laser pulses cannot be produced via the birefringent crystal, instead there is only a single beam of blue femtosecond laser irradiation. As a result, the typical 1D semi-periodic nanograting surface structures were observed to form, in accompany

with the poor quality of bending, splitting and interruption phenomena, being very similar to the situations in the previous reports [19]. In general, this is a great challenge for the application of surface photonic devices. On the other hand, when the azimuth angle of the crystal was clockwise rotated to α = 30°, we were able to obtain the double-beam femtosecond lasers with the energy fluence ratio of $F_1:F_2 = 3:1$, and consequently the quality of the nanograting structure formation was found to improve significantly with the highly uniform spatial distribution, as shown by the SEM images in Fig. 2(a). In this case the periodic grooves can be well organized in the mm^2 scale area without the previously observed distorting defects, which dramatically improves the spatial regularity of the surface structures in comparison with the result of single-beam femtosecond laser irradiation [39–40]. Moreover, the spatial orientation of the induced uniform nanograting surface structures is found perpendicular to the direction of the linear polarization of the high-fluenced laser beam E_1. The corresponding high resolution SEM image demonstrates that the grating ridges tend to possess the unprecedented straight and smooth features without wavy and splitting profiles. The measured grating period approximates $\Lambda = 260$ nm, associated with the groove width of $w = 100$ nm.

The spatial frequency image of the uniform nanograting structures was obtained using 2D Fast Fourier transformation (FFT) method, as displayed in Fig. 2(b). It is clear that the calculated discrete distribution of the frequencies line up in the direction perpendicular to the structure orientation, which also implies the excellent uniformity of the surface structures in the spatial domain. The retrieved data along the connection of frequencies (the white dot line in the middle) was plotted in Fig. 2(d), where an interval of approximately $f = 3.73$ μm^{-1} between the two adjacent frequency peaks indicates the reciprocal spatial period of 268 nm, being consistent with the measurement from the SEM image. The calculated dispersion in structure orientation angle (DSOA), which is used to quantitatively characterize the structures regularity [38], is about δθ = 6.5°, as shown in Fig. 2(e). This result also indicates the remarkable uniform formation of the structures on the material surface.

In fact, as we continuously clockwise rotated the azimuth angle of the birefringent crystal to α = 37°, which corresponds to the energy fluence ratio of $F_1:F_2 = 1.52$ between double laser pulses, another kind of surface structure was observed to form, as shown in Fig. 3(a). Much different from the observation of the 1D nanograting structures in Fig. 2, in this case the uniform formation of 2D arrays of nanoscale triangles can be unexpected to achieve, wherein the neighboring six nano-triangles were seen to organize into a hexagonal pattern, as shown by the yellow solid lines in the high resolution SEM image. Because the formation of triangle structure is indeed realized by the mutual cross-linking of three ablation grooves, which are oriented in the left-slanted, right-slanted and horizontal directions, respectively, the whole structure pattern can be understood as a result of the spatial interlocking of three groups of 1D nanogratings. Moreover, the left-slanted orientation of the grooves is seen perpendicular to the direction of the linear polarization of the high-fluenced laser E_1, while other two groove orientations are found neither parallel nor perpendicular to the linear polarizations of double laser pulses. The measured spatial periods for the three groups of the nanogratings with the left-slanted, right-slanted and horizontal orientations approximate $\Lambda_1 = 265$ nm,

Table 1
Summary of the LIPSSs formed on Mo surface.

| Material	Beam properties	Laser parameters	Environ-ment	Period	LIPSS Morphology	Regularity	Refs
Bulk	Single beam	800 nm, 160 fs, 10 Hz	Air	0.81λ	Grating	Bad	[34]
Bulk	Single beam	1045 nm, 700 fs, 100 kHz	Hexane	0.2 λ	Grating	Bad	[35]
Bulk	Single beam	800/400 nm, 110 fs, 1 kHz	Air, Water	0.66 λ, 0.42 λ	Grating, Nanopillars	Bad	[36]
Bulk	Single beam	1030 nm, 400 fs, 400 kHz	Air	0.74 λ	Triangular, Rhombic	Bad	[37]
Film	Single beam	1030 nm, 213 fs, 600 kHz,	Air	0.82 λ	Grating	Good	[38]
Bulk	Two-color beam	800 nm and 400 nm, 50 fs, 1 kHz, Δt = 100 ps	Air	0.75 λ	Dot array	Bad	[20]
Bulk	Two beam	400 nm, 40 fs, 1 kHz, Δt = 1.5 ps	Air	0.65λ ~ 0.85 λ	Grating, Triangle, Dot	Good	This work
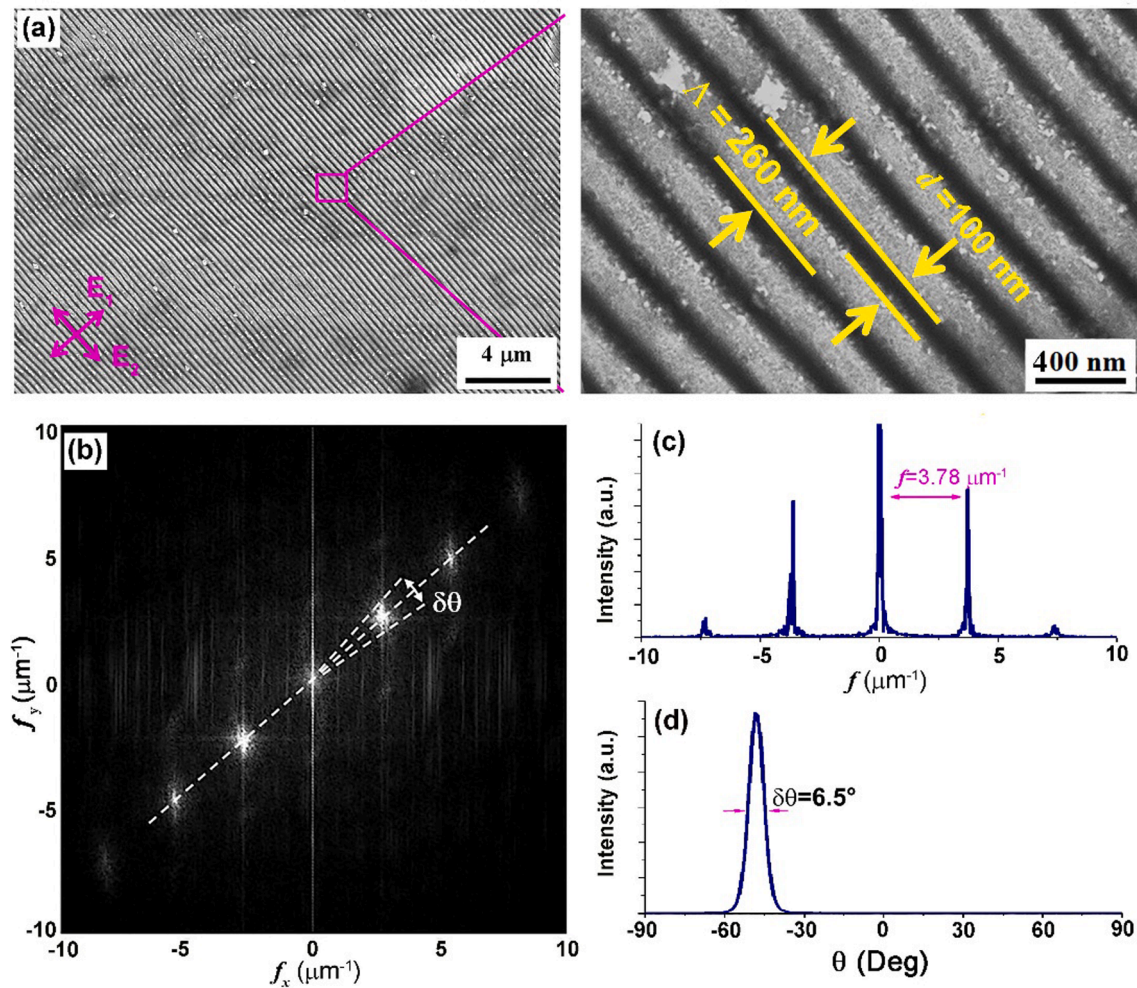
Fig. 2. Characterization of the uniform 1D nanograting surface structures on Mo surface induced by orthogonal polarizations of double femtosecond blue lasers with a time delay of 1.5 ps, where the energy fluence ratio between them is given by F_1: $F_2 = 3$:1 at the total laser fluence of F = 0.182 J/cm^2. (a)-(b) SEM and 2D-FFT images of the nanograting structures. (c) Retrieved distribution of the frequency components along the middle white dot line in (b). (d) Calculated curve of the structure orientation angle distribution.

$\Lambda_2 = 320$ nm and $\Lambda_3 = 340$ nm, respectively, and their ablation groove widths are $w_1 = 70$ nm, $w_2 = 60$ nm and $w_3 = 60$ nm, respectively. As for the nanotriangle structure unit, the measured three side lengths have the equal value of $l = 200$ nm. Likewise, the laser-induced nanotriangle structure arrays present the excellent uniform distribution and the high quality morphology of the structure unit within the sub-mm^2 even mm^2 scale area.

Fig. 3(b) displays the spatial frequency image of the 2D nanotriangle structure arrays using 2D-FFT, where the discrete frequency spots with a clear distribution feature were also arranged in the hexagonal pattern. The retrieved data along three chains of the frequency connection (white dot lines) are plotted in Fig. 3 (c)-(e), whose providing the sharp frequency peaks imply the remarkablely uniform distribution of the 2D nanotriangle structure arrays in the spatial domain. The measured intervals of $f_1 = 3.76$ μm^{-1}, $f_2 = 3.09$ μm^{-1} and $f_3 = 2.97$ μm^{-1} between the two adjacent frequency spots along three different alignment directions indicate the reciprocal spatial periods of 268 nm, 320 nm and 338 nm, respectively, which agree with the measurement results in the SEM images.

On the other hand, when the azimuth angle of the birefringent crystal was further rotated to $\alpha = 45°$, the double laser pulses are certain to possess the equal energy, or the energy fluence ratio reduces to F_1: $F_2 = 1$, and the available laser-induced surface structures turn to become the uniform distribution of 2D nanodot arrays, as shown in Fig. 4(a).

Similar to the aforementioned analyses, such structure pattern can be viewed as a result of the spatial interlocking of two groups of 1D nanogratings oriented in orthogonal directions, which are perpendicular to the linear polarizations of the double laser pulses, respectively. In particular, the formation of the highly uniform nanodot structure arrays can also be evidenced within the sub-mm^2 even mm^2 scale area with the high-quality structure unit. The measured spatial periods along the two grating orientations approximate $\Lambda_1 = 260$ nm and $\Lambda_2 = 290$ nm, associated with the groove width of $w_1 = 120$ nm and $w_2 = 150$ nm, respectively, resulting in a dot diameter of D = 140 nm. The calculated spatial frequency image for the 2D nanodot structure arrays, as shown in Fig. 4 (b), demonstrates the clear and discrete distribution of the frequencies in a square pattern. The narrow peaks in the retrieved data along the two chains of frequency connection (while dot lines), as shown in Fig. 4(c)-(d), hint the prominently uniform distribution of the nanodot structure arrays in the space domain. The measured frequency interval of $f_1 = 3.80$ μm^{-1} and $f_2 = 3.46$ μm^{-1} suggests the two reciprocal periods of 263 nm and 289 nm, being coincident with the measurement values in the SEM images.

3.2. EDS analysis

A chemical analysis of the pristine and femtosecond laser nano-structuring regions on Mo surface was performed by a comparative
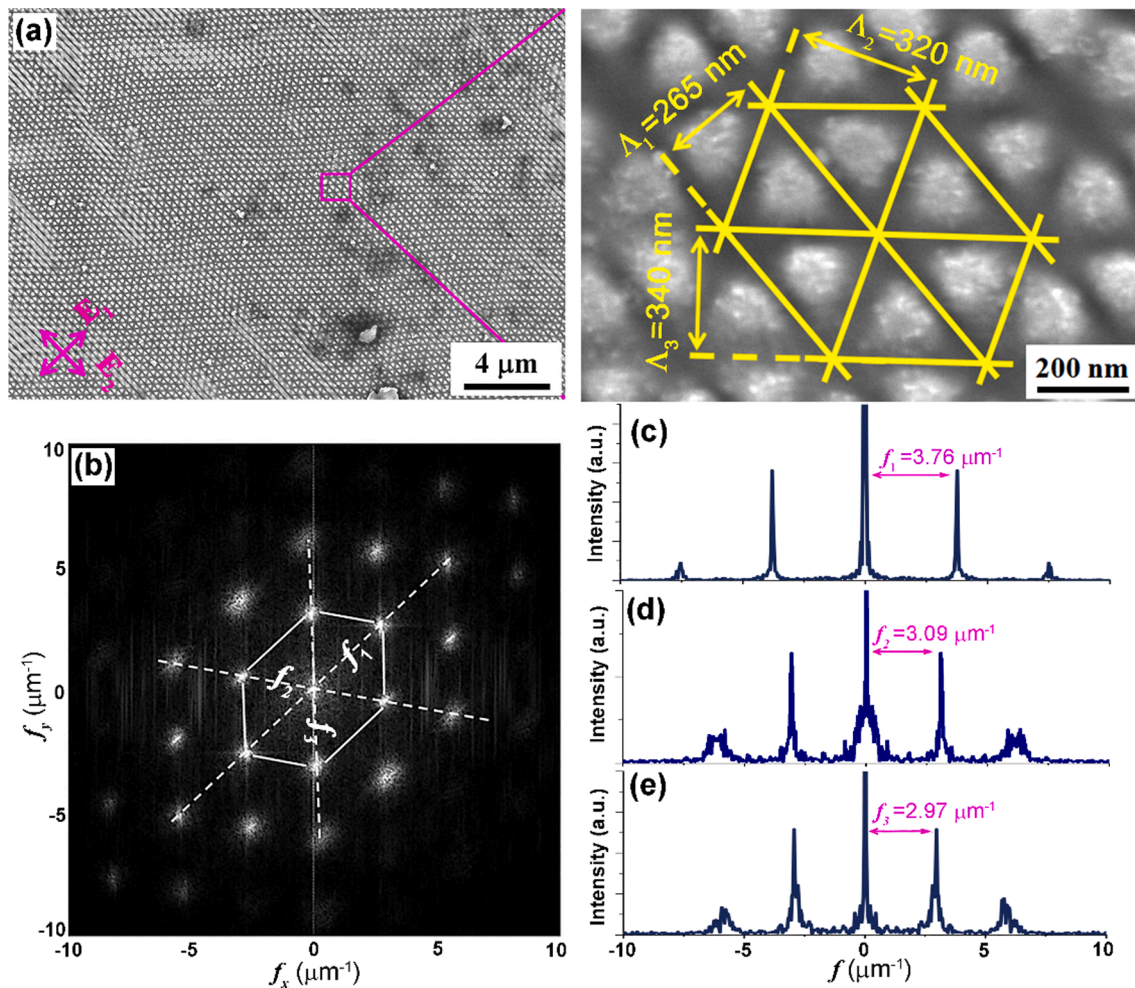
Fig. 3. Characterization of the uniform 2D arrays of nanoscale triangles surface structures on Mo surface induced by orthogonal polarizations of double femtosecond blue lasers with a time delay of 1.5 ps, where the energy fluence ratio between them is given by F_1: F_2 = 1.52: 1 with the total fluence of F = 0.182 J/cm². (a)-(b) SEM and 2D-FFT images of the nanotriangle structures; (c)-(e) Retrieved distributions of the frequency components along the three white dot lines in (b).

study of energy-dispersive X-Ray spectroscopy (EDS), as illustrated in Table 2. Appearing oxygen (O) element on the pristine Mo surface can be ascribed to the formation of native molybdenum trioxide (MoO$_3$) layer in air [41]. After the femtosecond laser nanostructuring of Mo, the weight concentration of oxygen (O) element is observed to increase from 5.76% to 7.42% due to the generation of new Mo oxides [41], while it decreases from 94.24% to 92.58% for Mo element. This result demonstrates that the laser-induced surface nanostructures are mainly composed of Mo and doped with a small amount of Mo oxides.

3.3. Dynamic window of the surface nanostructures formation

In addition, we carried out massive experiments with varying the laser parameters to investigate the formation of the three types of highly regular surface structures. It was found that the appropriate scanning velocities were located within a narrow range of $v = 0.01 \sim 0.02$ mm/s, and the valid defocusing distance of the sample surface can be varied in a range of $s = 200 \sim 400$ μm. With the selected scanning speed of $v = 0.01$ μm/s and the defocusing distance of $s = 250$ μm, we experimentally obtained the dynamic windows for the formation of three uniform surface structures, in terms of the totally incident laser fluence and the energy fluence ratio (F_1: F_2) between the double laser pulses, as illustrated in Fig. 5. Clearly, when the laser energy ratio values are given within two ranges of $1:3 < F_1:F_2 < 2:3$ and $3:2 < F_1:F_2 < 3$, the homogeneous 1D nanograting structures can be achieved; whereas for the variation of the laser energy ratio within two ranges of $0.5 < F_1:F_2 < 0.8$

and $1.25 < F_1:F_2 < 2$, the homogeneous 2D nanotriangle structure arrays can be formed; however, the laser fluence ratios for producing the homogeneous 2D nanodot structure arrays are found to confine within a range of $0.8 < F_1:F_2 < 1.25$. Here, a "symmetric" behavior is observed for the three nanostructures formation with respect to the energy ratios of F_1/F_2 and F_2/F_1, which means they are determined by the relative energy fluence ratio and independent on the incidence order of double pulses in time sequence. Moreover, the proper energy fluence ratios for the formation of three homogeneous surface structures seem to rely on the total laser fluence. The higher the total incident laser fluence, the narrower the valid range becomes. Otherwise, either the irregular or no surface structures was formed.

3.4. Physical origins of the surface nanostructures formation

As reported in the previous studies [42–43], the laser-induced nanograting surface structures stem from the excited surface plasmon polaritons (SPP) whose subsequent interference with the incident laser gives rise to the intensity fringes on the material surface. The response of the material surface following the energy deposition often undergoes a series of ultrafast dynamic processes, which involve the optical absorption by free electrons, the energy transfer from electron to the lattice subsystems, the melting, hydrodynamics and re-solidification of the lattice [14–16]. During the initial stage, the absorption of the periodic laser energy fringes was memorized by the material surface in a form of transient refraction index grating (TRIG) patterns, which consequently
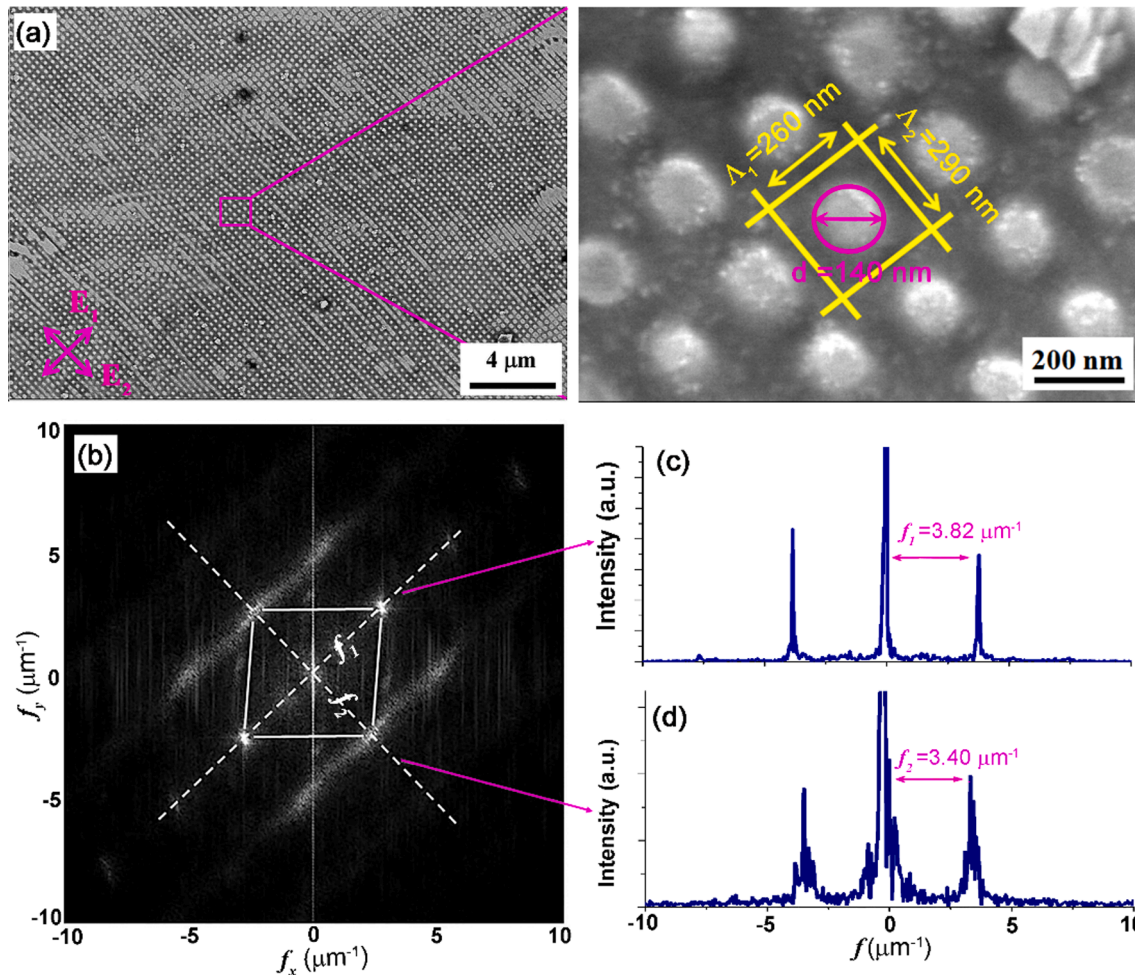
Fig. 4. Characterization of the uniform 2D arrays of nanoscale dots surface structure on Mo surface induced by orthogonal polarizations of double femtosecond blue lasers with a time delay of 1.5 ps, where the energy fluence ratio between them is given by $F_1: F_2 = 1:1$ with the total incident laser fluence of $F = 0.182$ J/cm^2. (a)-(b) SEM and 2D-FFT images of the nanodot structures. (c)-(d) Retrieved distributions of the frequency components along the two white dot lines in (b).

Table 2
Chemical analysis of the pristine and femtosecond laser nanostructuring regions on Mo surface.

Elements	Pristine (wt. %)	Nanostructuring (wt. %)
Mo	5.76	7.42
O	94.24	92.58

causes the spatial selection of the material removal for the permanent nanograting structures. In practice, the well-arranged surface structures were generally developed by the multi-pulse exposure, wherein a positive inter-pulse feedback between the laser-exposed surface morphology and the SPP excitation is established [1,39–40]. Based on such a feedback mechanism, the laser-exposed surface morphology begins to evolve from the random nanostructures into the nascent periodic patterns, finally resulting in the well-defined surface structures. During these processes, the grating-assisted coupling between the laser and the excited SPPs tends to gradually convert from the nonresonant mode into the resonant mode with the evolution of the surface morphology. By taking into account the predominant role of the SPP excitation in the nanograting structure formation, the generation of three types of highly regular surface structures that consist of one, two and three groups of nanogratings can be ascribed to the excitation of the single, double and three SPPs with different wave vectors, respectively. The time delay of 1.5 ps between the double laser pulses, being shorter than the electron-lattice coupling time (~10 ps) in metals, makes the dual dynamic

processes of the laser-material interactions mutually correlated in the transient non-equilibrium conditions. Next, we will establish the physical scenarios for the single, double and three SPPs excitations based on the dynamic correlation effects, to explain the formation of the highly regular surface structures.

The sketches in the middle raw of Fig. 6 illustrate a physical description for the single SPP excitation on molybdenum material upon irradiation of double femtosecond lasers with the energy fluence ratio of $F_1:F_2 = 3$, which corresponds to the formation of the highly regular nanograting structures. Owing to the large difference between the two energy fluences, the strong SPP excitation of the incident laser pulse with the relatively high energy is ready to predominate the emergence of the nascent nanograting structures, while the irradiation of the laser pulse with the relatively low energy is inclined to heat the material surface. In other words, such different contributions from the double femtosecond laser pulses to the nascent grating development are actually determined by their energy fluences regardless of the time-sequential incidence. As a result, the spatial orientation of the nascent grating patterns becomes perpendicular to the direction of the linear polarization of the laser pulse with the high energy. When the follow-up laser pulse pairs with orthogonal linear polarizations are incident on the nascent grating patterned surface, the high-energy laser pulse is logically regarded as the TM polarization whereas the low-energy laser pulse as the TE polarization, and their energy depositions on the nascent grating patterns can be simulated using the finite-difference time-domain (FDTD) method, as shown in Fig. 6 (c). Here, the geometric
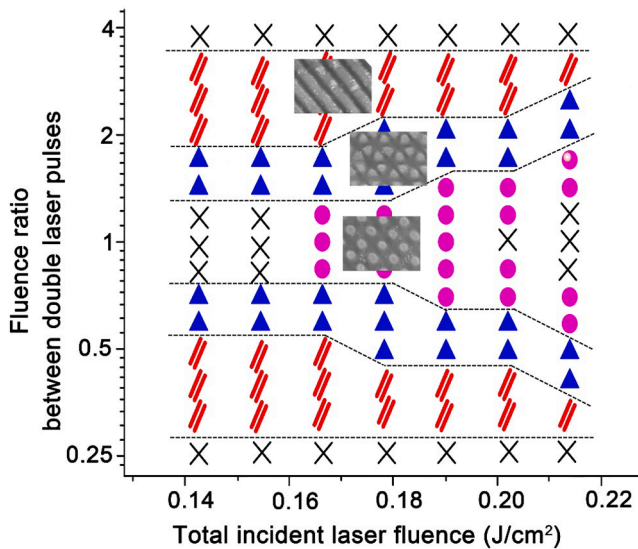
Fig. 5. Experimentally obtained a dynamic window for the switchable formation of three types of highly regular nanostructures on Mo surface, in term of the total incident laser fluence and the fluence ratio between double laser pulses, where the symbols of '//', '▲', and '●' represent the corresponding structure formations like the inset SEM images, and the symbol of '×' for the irregular or no structure formation. The scanning speed and the defocused distance are fixed at $v = 0.01$ mm/s and $s = 250$ μm, respectively.

parameters of the structure design are provided by $\Lambda = 260$ nm, $w = 80$ nm and $d = 60$ nm on the basis of the experimental measurements, while the permittivity of Mo material is assumed as $\varepsilon = -1.64 + i1$ at the wavelength of $\lambda = 400$ nm by considering the surface modification from the multi-pulse exposure. Clearly, for the incident TM-polarized light the calculated electromagnetic (EM) field intensity is enhanced on the grating ridge areas, leading to the ridge-center-preference energy deposition; while for the incident TE-polarized light the calculated enhancement of the EM field is concentrated around two edges of the groove, leading to the groove-edge-preference energy deposition.

During the multi-pulse exposure of single-beam laser irradiation, the follow-up light incidence should be always deemed as the TM-polarization, so that there is only the ridge-center-preference energy deposition on the nascent grating patterns, which unavoidably results in the ridge splitting effect to deteriorate the spatial arrangement of the structures [39–40]. In contrast, for the case of double laser pulses irradiation the two different EM field enhancement behaviors from both the TM and TE-polarized laser pulses can take place, and their spatial counterbalance tends to achieve the nearly homogeneous energy deposition on the nascent grating surface, which not only makes the ridge splitting suppressed but also causes the smoothness of the structure. As a result, the positive feedback is constituted to regulate the growth of the nascent grating patterns with multi-pulse-pair exposures, thus finally leading to the large-area uniform distribution of the nanograting structures.

When the energy fluence ratio of the double laser pulses is decreased to $F_1:F_2 = 1.7:1$, the physical picture for the excitation of three SPPs is diagramed in the bottom raw of Fig. 6, which devotes to interpreting the formation of the regular 2D nanotriangle structure arrays. At the early stage of the nascent grating formation, the high-energy laser pulse is ready to generate the $TRIG_1$ pattern (with a reciprocal lattice vector $|\vec{k}_{TRIG1}| = 2\pi/\Lambda_1$) via its SPP excitation regardless of the first or time-delayed incidence, which finally evolves into one group of the nascent grating with orientation perpendicular to its polarization direction. Much different from the situation with the energy fluence ratio of $F_1:F_2 = 3:1$, in this case the physical contribution of the low-energy laser

pulse to the morphology of the nascent grating surface becomes no longer negligible, its interplay with the $TRIG_1$ pattern will modulate the structure morphology.

When the high energy of laser pulse E_1 reaches the target at first in the time sequence, the delayed incident low energy of laser pulse E_2 is deemed to couple with the existing $TRIG_1$ pattern, as shown in Fig. 6(d). The Gaussian intensity profile of the first laser pulse spot results in a gradient refraction index profile for the optically modified layer with the maximum change in the center of the Gaussian laser spot, which modulates the whole profile of the $TRIG_1$ pattern, as shown by the blue curve profiles in Fig. 6(b), 6(d) and 6(g). When incident on the gradient-index $TRIG_1$ pattern, the delayed incident laser pulse E_2 tends to be deflected from the normal incidence with a deflection angle of θ, as shown by the inset in Fig. 6(d). Under such circumstances, the tangential component of the deflected light can non-collinearly make two SPPs (SPP$_2$, SPP$_3$) excitation on the optically modified surface by scattering of the $TRIG_1$ pattern [44], whose wave vectors satisfy the phase matching condition $\vec{k}_{spp2,3} = n\vec{k}_0\sin\theta \pm \vec{k}_g$, where $\pm\vec{k}_g$ is an additional vector provided by the $TRIG_1$ pattern for compensating the difference between $n\vec{k}_0\sin\theta$ and $\vec{k}_{spp2,3}$. The noncollinear excitation of the two SPPs was simulated by the FDTD method, as shown in Fig. 6(e), where the structure design for the $TRIG_1$ pattern was the same as that in Fig. 6(c). In the vectorial diagram of the two noncollinear SPPs excitation in the plane of the $TRIG_1$ surface, the propagation directions for the two SPPs are determined by the azimuth angle of $\varphi_{2,3} = \pm\cos^{-1}(|n\vec{k}_0\sin\theta|/|\vec{k}_{spp2,3}|)$ with respect to the $TRIG_1$ orientation.

Noting that, the magnitude of $\vec{k}_{spp2,3}$ depending on the permittivity of sample material remains unchanged. The magnitude of $n\vec{k}_0\sin\theta$ is mainly proportional to the energy fluence of the time delayed laser pulse E_2. With increasing the laser pulse fluence, $n\vec{k}_0\sin\theta$ becomes higher in the magnitude, so that the azimuth angle of $\varphi_{2,3}$ decreases and $\vec{k}_g$ reduces in the magnitude accordingly. The resonance excitation for two noncollinear SPPs with the high efficiency is supposed to occur when $\vec{k}_g$ is half of $\vec{k}_{TRIG1}$ in the magnitude, that is, the three vectors of $\vec{k}_{spp2}$, $\vec{k}_{spp3}$ and $\vec{k}_{TRIG1}$ construct a quasi-equilateral triangle due to their approximately equal magnitudes, as shown by the pink and yellow solid lines in Fig. 6(d), since the phase matching condition is fully fulfilled. Moreover, the two noncollinear SPPs can be resonantly diffracted by the $TRIG_1$ pattern to each other: $\vec{k}_{spp2} \pm \vec{k}_{TRIG1} = \vec{k}_{spp3}$. At this case, the azimuth angle $\varphi_{2,3}$ for the two noncollinearly excited SPPs is approximately $\pm 30°$. In our experiments, the resonance excitation of the two noncollinear SPPs was verified to occur within the energy-fluence-ratio range of $1.4 < F_1:F_2 < 1.7$ for the double laser pulses. In other energy-fluence-ratios, the non-resonance excitation of the two non-collinear SPPs at other azimuth angles is negligible for the structure morphology formation due to low efficiency. Likewise, the interference of the low-energy laser pulse E_2 with the two non-collinear SPPs at the azimuth angle of $\varphi_{2,3}=\pm30°$ will lead to two other groups of the nascent grating patterns, with a deflecting orientation angle of $\pm 60°$ relative to the precedent nascent grating patterns. Therefore, their spatially mutual interlockings would like to form the nascent 2D nanotriangle structure arrays, where the two groups of the grooves induced by the low-energy laser pulse apparent to have the shallower depth than that induced by the high-energy laser pulse.

With the continuous pulse-pair exposure on the nascent 2D nanotriangle structure arrays, as shown in Fig. 6(f), the high-energy laser pulse E_1 is capable of exciting three SPPs in the noncollinear directions, while the two noncollinear SPPs excited by the low-energy laser pulse E_2 are ready to propagate normal to the two groups of periodic grooves with the shallow depth. The excited three SPPs can further facilitate the growth of the existing nascent structure arrays by localizing the double laser energies into the grooves, and vice versa. As a result, the positive
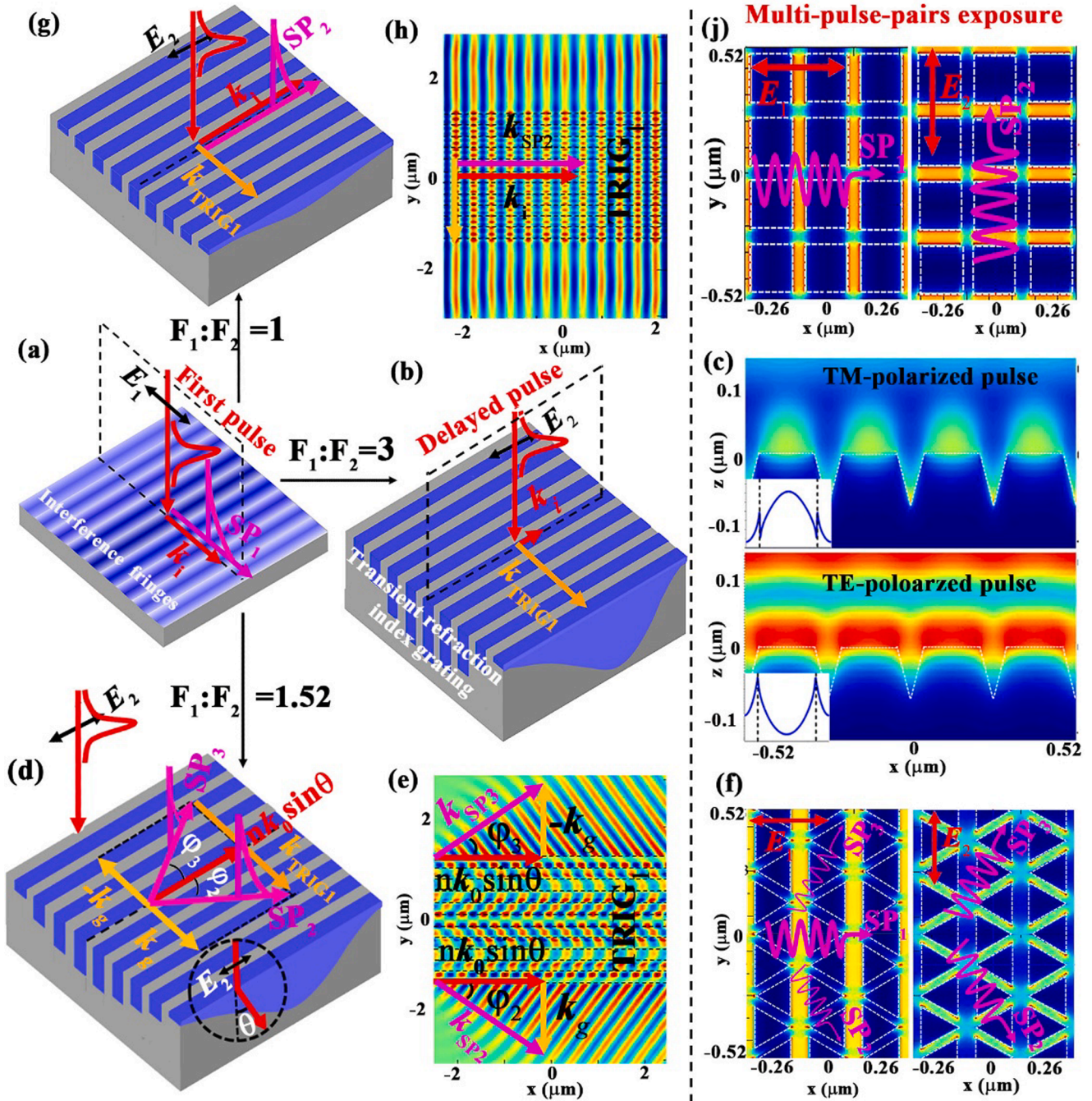
Fig. 6. Proposed physical scenarios for the formation of three types of highly regular surface structures upon irradiation of double time-delayed femtosecond lasers with orthogonal linear polarizations. (a) Schematic of the spatially periodic energy distribution on molybdenum surface dominated by the first incident laser pulse E_1 via the collinear excitation of SP_1, to which the response of the material brings the transient refraction index gratings ($TRIG_1$, shaded blue regions in (b), (d), (g)) and the convex-lens-like optically modulated thin layer (the profile of $TRIG_1$); (b) Schematic of null SPP excitation on the existing $TRIG_1$ under the time-delayed laser pulse E_2 irradiation with the energy fluence ratio of $F_2: F_1 = 1:3$; (c) Simulated spatial distributions of the electromagnetic (EM) field on the V-shaped nascent nanograting structure with exposure of multi-pulse-pairs of orthogonal polarizations, i.e., both the transverse magnetic (TM) and the transverse electric (TE) polarized lights, insets for the profiles on the transverse plane of the groove surface; (d) Schematic of noncollinear excitation of SP_2 and SP_3 on the existing $TRIG_1$ under the laser pulse E_2 irradiation with the energy fluence ratio of $F_2: F_1 = 1:1.7$, and the inset for the light deflection behavior of the laser pulse E_2 inside the convex-lens-like optically modulated thin layer; (e) Simulated EM field distribution of the two non-collinearly excited SPPs; (f) Simulated SPPs excitation on the nascent 2D triangle structure arrays with multi-pulse-pairs exposure; (g) Schematic of collinear excitation of SP_2 under the laser pulse E_2 irradiation with the energy fluence ratio of $F_2: F_1 = 1:1$; (h) Simulated EM field distribution of the collinearly excited SP_2; (j) Simulated SPPs excitation on the nascent 2D nanodot structure arrays with multi-pulse-pairs exposure.

feedback is constituted to regulate the growth of the nascent 2D nano-triangle structures with multi-pulse-pair exposures, thus finally leading to a long-range uniform distribution of the surface structures.

On the other hand, when the low energy of laser pulse reaches the

target at first, the incident time-delayed high energy of laser pulse is responsible for producing one group of nascent grating via smearing out the TRIG pattern induced by the low-energy laser pulse. Under the subsequent pulse-pair irradiation, the temporally first incident low-

energy laser pulse is ready to deflect by the optically modified surface, and subsequently causes two noncollinear propagation of SPP excitations, finally leading to another two groups of nascent gratings. Such nascent structures can constitute the positive feedback mechanism with the excitation of three SPPs, and gradually evolve into the highly regular 2D nanotriangle structures under the continuous exposure of multiple double laser pulses.

The diagram in the top raw of Fig. 6 depicts the physical scenario of the two SPPs excitation based on double-laser irradiation with the energy fluence ratio close to $F_1:F_2 = 1:1$, which corresponds to the formation of the highly regular 2D nanodot structure arrays. At the birth stage of the nascent grating surface, the temporally first incident laser pulse E_1 brings forth the pattern of $TRIG_1$ via the collinear excitation of SPP_1. Because the decreased energy fluence of the laser pulse E_1 tends to minish the depth of the $TRIG_1$ pattern and flatten the gradient-index $TRIG_1$ profile, both the scattering and deflection of the $TRIG_1$ pattern for the temporally delayed incident laser pulse E_2 begin to vanish. Under this circumstance, the laser pulse E_2 can excite SPP_2 independently and collinearly to generate another $TRIG_2$ pattern, as demonstrated by the simulated EM field distribution in Fig. 6(g). The spatial interlocking between the two TRIG patterns is doomed to produce the nascent 2D nanocube structure arrays. With succeeding multi-pulse-pair exposures, both the growth of the 2D existing nascent arrays and the excitation of double SPPs are constructively feed each other, as shown in Fig. 6(i), finally resulting in the uniform formation of large-area 2D nanodot structure arrays with the thermal melting at the corners of the structure units.

3.5. Potential applications

A large-area nanograting pattern has been demonstrated to not only produce good monochromaticity of the structural colors for the short-wavelength visible lights but also display excellent broadband antireflection performances in the wavelength range of 400–1000 nm for the TM-polarized light incidence [19]. When compared with the nanogratings, it is conceivable that the large-area 2D nanotriangle and nanodot structures could generate the same antireflection performance for the polarized and unpolarized light incidence, and produce the same structural colors along three or two directions [45]. Furthermore, the nanostructured Mo surface with oxidization can be used as the high-efficiency substrates for the second-harmonic generation signal [46] and surface-enhanced Raman spectroscopy via the oxygen-vacancy correlated localized surface plasmon resonance (LSPR) effect [47]. Beyond those applications, the nanostructured Mo surface enables other numerous potential applications on wettability modification [48], antifriction [49], photoelectron enhancement [50], thermal management [51], etc.

4. Conclusions

We demonstrate a strategy for the controllable nanostructuring of molybdenum surface with large-area uniform periodic nanostructures using cylindrical focusing of double time-delayed femtosecond blue lasers with orthogonal linear polarizations. Three types of the surface nanostructures, featuring nanograting, nanotriangle and nanodot structure arrays, are controllably manufactured by the proper choice of the energy fluence ratios between the double laser pulses, respectively. The achieved surface structures can decrease down to 140 nm and 260 nm in the structural size and spatial period. The microscopic observations combining with Fourier frequency analysis demonstrate that the nanostructures present the extremely long-range uniform distribution and the high quality morphology of the structure unit. The switchable formation conditions for the three types of nanostructures were experimentally obtained with respect to the total energy fluence and the double laser fluence ratios. Taking the standard SPP model of LIPSSs into account, the physical origins of the nanostructures were

ascribed to the multiple surface plasmon excitations during the temporally correlated dynamic processes of the dual laser-material interactions. Our investigations facilitate the efficient scale-up manufacturing of 2D nanoscale surface structures, promising potential applications in the nanoscience fields of photonic crystal, nanoplasmonics, nanotribology, nanofluidic, etc.

CRediT authorship contribution statement

Bo Zhao: Conceptualization, Investigation, Writing – original draft. **Xiaofang Zhou:** Writing – review & editing. **Xin Zheng:** Methodology. **Ruiping Wang:** Formal analysis. **Yucai Lin:** Data curation. **Tingting Zou:** Software. **Zhenfen Huang:** Visualization, Formal analysis. **Changming Huang:** Writing – review & editing. **Jianjun Yang:** Writing – review & editing, Funding acquisition, Project administration, Supervision.

Declaration of Competing Interest

The authors declare that they have no known competing financial interests or personal relationships that could have appeared to influence the work reported in this paper.

Acknowledgements

References

[1] J. Bonse, S. Hohm, S.V. Kirner, A. Rosenfeld, J. Kruger, Laser-induced periodic surface structures - a scientifc evergreen, IEEE J. Sel. Top. Quantum Electron. 23 (2017) 9000615, https://doi.org/10.1109/JSTQE.2016.2614183.

[2] R. Stoian, J. Colombier, Advances in ultrafast laser structuring of materials at the nanoscale, Nanophotonics 9 (2020) 4665–4688, https://doi.org/10.1515/nanoph-2020-0310.

[3] H. Xie, B. Zhao, J. Cheng, C.S. Kumar, T. Zou, W. Xin, J. Yang, Super-regular femtosecond laser nanolithography based on dual-interface plasmons coupling, Nanophotonics 10 (15) (2021) 3831–3842, https://doi.org/10.1515/nanoph-2021-0329.

[4] Y.H. Liu, Y.K. Tseng, C.W. Cheng, Direct fabrication of rotational femtosecond laser-induced periodic surface structure on a tilted stainless steel surface, Opt. Laser Technol. 134 (2021), 106648, https://doi.org/10.1016/j.optlastec.2020.106648.

[5] T. Zou, B. Zhao, W. Xin, F. Wang, H. Xie, Y. Li, Y. Shan, K. Li, Y. Sun, J. Yang, Birefringent response of graphene oxide film structurized via femtosecond laser, Nano Res. 15 (2022) 4490–4499, https://doi.org/10.1007/s12274-021-3505-x.

[6] P.G. Blauner, Focused ion beam fabrication of submicron gold structures, J. Vac. Sci. Technol. B 7 (4) (1989) 609, https://doi.org/10.1116/1.584803.

[7] M. Imboden, D. Bishop, Top-down nanomanufacturing, Phys. Today 2014 67(12) (2014) 45–50. https://doi.org/10.1063/PT.3.2621.

[8] S.P. Murzin, G. Liedl, R. Pospichal, Coloration of a copper surface by nanostructuring with femtosecond laser pulses, Opt. Laser Technol. 119 (2019), 105574, https://doi.org/10.1016/j.optlastec.2019.105574.

[9] H.C. Yuan, V.E. Yost, M.R. Page, P. Stradins, D.L. Meier, H.M. Branz, Efficient black silicon solar cell with a density-graded nanoporous surface: optical properties, performance limitations, and design rules, Appl. Phys. Lett. 95 (12) (2009), 123501, https://doi.org/10.1063/1.3231438.

[10] V. Zorba, L. Persano, D. Pisignano, A. Athanassiou, E. Stratakis, R. Cingolani, P. Tzanetakis, C. Fotakis, Making silicon hydrophobic: wettability control by two-length scale simultaneous patterning with femtosecond laser irradiation, Nanotechnology 17 (13) (2006) 3234–3238, https://doi.org/10.1088/0957-4484/17/13/026.

[11] J. Bonse, R. Koter, M. Hartelt, D. Spaltmann, S. Pentzien, S. Hohm, A. Rosenfeld, J. Krüger, Femtosecond laser-induced periodic surface structures on steel and titanium alloy for tribological applications, Appl. Phys. A 117 (1) (2014) 103–110, https://doi.org/10.1007/s00339-014-8229-2.

[12] N. Liu, Y. Sun, H. Wang, C. Liang, Femtosecond laser-induced nanostructures on Fe-30Mn surfaces for biomedical applications, Opt. Laser Technol. 139 (2021), 106986, https://doi.org/10.1016/j.optlastec.2021.106986.

[13] J. Bonse, S. Graf, Maxwell meets marangoni—a review of theories on laser-induced periodic surface structures", Laser Photonics Rev. 14 (10) (2020) 2000215, https://doi.org/10.1002/lpor.202000215.

[14] K. Cheng, K. Cao, Y. Zhang, R. Han, D. Feng, J. Liu, S. Zhang, Z. Sun, T. Jia, Ultrafast dynamics of subwavelength periodic ripples induced by single femtosecond pulse: from noble to common metals, J. Phys. D: Appl. Phys. 53 (28) (2020), 285102, https://doi.org/10.1088/1361-6463/ab82d9.

[15] M. Garcia-Lechuga, D. Puerto, Y. Fuentes-Edfuf, J. Solis, J. Siegel, Ultrafast moving-spot microscopy: Birth and growth of laser-induced periodic surface structures, ACS Photonics 3 (10) (2016) 1961–1967, https://doi.org/10.1021/acsphotonics.6b00514.

[16] R.D. Murphy, B. Torralva, D.P. Adams, S.M. Yalisove, Pump-probe imaging of laser-induced periodic surface structures after ultrafast irradiation of Si, Appl. Phys. Lett. 103 (2013), 141104, https://doi.org/10.1063/1.4823588.

[17] G. Giannuzzi, C. Gaudiuso, C.D. Franco, G. Scamarcio, P.M. Lugar'a, A. Ancona, Large area laser-induced periodic surface structures on steel by bursts of femtosecond pulses with picosecond delays, Opt. Laser. Eng. 114 (2019) 15–21. https://doi.org/10.1016/j.optlaseng.2018.10.006.

[18] B. Zhao, X. Zheng, Y. Lei, H. Xie, T. Zou, G. Yuan, W. Xin, J. Yang, High-efficiency-and-quality nanostructuring of molybdenum surfaces by orthogonally polarized blue femtosecond lasers, Appl. Surf. Sci. 572 (2022) 151371, https://doi.org/10.1016/j.apsusc.2021.151371.

[19] W. He, J.Y. Yang, C. Guo, Controlling periodic ripple microstructure formation on 4H-SiC crystal with three time-delayed femtosecond laser beams of different linear polarizations, Opt. Express 25 (5) (2017) 5156–5168, https://doi.org/10.1364/OE.25.005156.

[20] J. Cong, J. Yang, B. Zhao, X. Xu, Fabricating subwavelength dot-matrix surface structures of Molybdenum by transient correlated actions of two-color femtosecond laser beams, Opt. Express 23 (4) (2015) 5357–5367, https://doi.org/10.1364/OE.23.005357.

[21] H. Qiao, J. Yang, J. Li, Q. Liu, J. Liu, C. Guo, Formation of Subwavelength Periodic Triangular Arrays on Tungsten through Double-Pulsed Femtosecond Laser Irradiation, Materials 11 (2018) 2380, https://doi.org/10.3390/ma11122380.

[22] H. Qiao, J. Yang, F. Wang, Y. Yang, J. Sun, Femtosecond laser direct writing of large-area two-dimensional metallic photonic crystal structures on tungsten surfaces, Opt. Express 23 (2015) 26617–26627, https://doi.org/10.1364/OE.23.026617.

[23] Q. Liu, N. Zhang, J. Yang, H. Qiao, C. Guo, Direct fabricating large-area nanotriangle structure arrays on tungsten surface by nonlinear lithography of two femtosecond laser beams, Opt. Express **26**(9) (2018, 2018,) 11718–11727.

[24] M. Wang, N. Zhang, S.C. Chen, Effects of supra-wavelength periodic structures on the formation of 1D/2D periodic nanostructures by femtosecond lasers, Opt. Laser Technol. 151 (2022), 108058, https://doi.org/10.1016/j.optlastec.2022.108058.

[25] N. Zhang, S. Chen, Formation of nanostructures and optical analogues of massless Dirac particles via femtosecond lasers, Opt. Express 28 (24) (2020) 36109–36121, https://doi.org/10.1364/OE.403336.

[26] X. Zheng, B. Zhao, J. Yang, Y. Lei, T. Zou, C. Guo, Noncollinear excitation of surface plasmons for triangular structure formation on Cr surfaces by femtosecond lasers, Appl. Surf. Sci. 507 (2020), 144932, https://doi.org/10.1016/j.apsusc.2019.144932.

[27] Z. Zhao, B. Zhao, Y. Lei, J. Yang, C. Guo, Laser-induced regular nanostructure chains within microgrooves of Fe-based metallic glass, Appl. Surf. Sci. 529 (2020), 147156, https://doi.org/10.1016/j.apsusc.2020.147156.

[28] B. Dromey, M. Zepf, M. Landreman, K. O'Keeffe, T. Robinson, S.M. Hooker, Generation of a train of ultrashort pulses from a compact birefringent crystal array, Appl. Opt. 46 (22) (2007) 5142–5146, https://doi.org/10.1364/AO.46.005142.

[29] A.K. Sharma, J. Smedley, T. Tsang, T. Rao, Formation of subwavelength grating on molybdenum mirrors using a femtosecond Ti:sapphire laser system operating at 10 Hz, Rev. Sci. Instrum. 82 (3) (2011), 033113, https://doi.org/10.1063/1.3569763.

[30] A. Voznesenskaya, D. Kochuev, A. Zhdanov, Research on the tribological properties of periodic micro- and nanostructures on the molybdenum surface obtained as a result of laser action, Mater. Today Proc. 19 (5) (2019) 1–4, https://doi.org/10.1016/j.matpr.2019.07.069.

[31] J. Wang, C. Guo, Numerical study of ultrafast dynamics of femtosecond laser induced periodic surface structure formation on noble metals, J. Appl. Phys. 102 (5) (2007), 053522, https://doi.org/10.1063/1.2776004.

[32] S. Bashir, M.S. Rafique, C.S. Nathala, A.A. Ajami, W. Husinsky, Femtosecond laser fluence based nanostructuring of W and Mo in ethanol, Physica B 513 (2017) 48–57, https://doi.org/10.1016/j.physb.2017.03.008.

[33] M. Hashida, Y. Ikuta, Y. Miyasaka, S. Tokita, S. Sakabe, Simple formula for the interspaces of periodic grating structures self-organized on metal surfaces by femtosecond laser ablation, Appl. Phys. Lett. 102 (2013), 174106, https://doi.org/10.1103/PhysRevB.82.165417.

[34] K. Okamuro, M. Hashida, Y. Miyasaka, Y. Ikuta, S. Tokita, S. Sakabe, Laser fluence dependence of periodic grating structures formed on metal surfaces under femtosecond laser pulse irradiation, Phys. Rev. B 82 (2010), 165417.

[35] Y. Tanaka, X. Yu, S. Terakawa, T. Ishida, K. Saitoh, H. Zhang, T. Asaka, F. Itoigawa, M. Kuwahara, S. Ono, Carbonization of a Molybdenum Substrate Surface and Nanoparticles by a One-Step Method of Femtosecond Laser Ablation in a Hexane Solution, ACS Omega 8 (8) (2023) 7932–7939, https://doi.org/10.1021/acsomega.2c07697.

[36] M.H. Dar, N.A. Saad, C. Sahoo, S.R.G. Naraharisetty, N.R. Desai, Ultrafast laser-induced reproducible nano-gratings on a molybdenum surface, Laser Phys. Lett. 14 (2017), 026101, https://doi.org/10.1088/1612-202X/aa5129.

[37] D. Zhang, R. Liu, Z. Li, Irregular LIPSS produced on metals by single linearly polarized femtosecond laser, Int. J. Extrem. Manuf. 4 (2022), 015102, https://doi.org/10.1088/2631-7990/ac376c.

[38] I. Gnilitskyi, J.Y. Derrien, Y. Levy, N.M. Bulgakova, M. Toma, L. Orazi, High-speed manufacturing of highly regular femtosecond laser-induced periodic surface structures: physical origin of regularity, Sci. Rep. 7 (2017) 8485, https://doi.org/10.1038/s41598-017-08788-z.

[39] M. Huang, Y. Cheng, F. Zhao, Z. Xu, The significant role of plasmonic effects in femtosecond laser-induced grating fabrication on the nanoscale, Ann Phys-Berlin 525 (1–2) (2013) 74–86, https://doi.org/10.1002/andp.201200136.

[40] J.W. Yao, C.Y. Zhang, H.Y. Liu, Q.F. Dai, L.J. Wu, S. Lan, A.V. Gopal, V. A. Trofimov, T.M. Lysak, High spatial frequency periodic structures induced on metal surface by femtosecond laser pulses, Opt. Express 20 (2) (2012) 905–911, https://doi.org/10.1364/OE.20.000905.

[41] L. Kotsedi, P. Mthunzi Z.Y. Nuru, S.M. Eaton, P. Sechoghela, N. Mongwaketsi R. Ramponi MMaaza. Femtosecond laser surface structuring of molybdenum thin films. Appl. Surf. Sci. 353 (2015) 1334-1341. https://doi.org/10.1016/j.apsusc.2015.08.047.

[42] J. Bonse, A. Rosenfeld, J. Krüger, On the role of surface plasmon polaritons in the formation of laser-induced periodic surface structures upon irradiation of silicon by femtosecond-laser pulses, J. Appl. Phys. 106 (10) (2019), 104910, https://doi.org/10.1063/1.3261734.

[43] M. Huang, F. Zhao, Y. Cheng, N. Xu, Z. Xu, Origin of Laser-induced near subwavelength ripples: interference between surface plasmons and incident laser, ACS Nano 3 (12) (2019) 4062–4070, https://doi.org/10.1021/nn900654v.

[44] A.V. Andreev, M.M. Nazarov, I.R. Prudnikov, A.P. Shkurinov, P. Masselin, Noncollinear excitation of surface electromagnetic waves: Enhancement of nonlinear optical surface response, Phys. Rev. B 69 (2004), 035403, https://doi.org/10.1103/PhysRevB.69.035403.

[45] W. Liu, J. Sun, J. Hu, L. Jiang, J. Huang, Z. Li, Z. Qiu, H. Liu, C. Li, X. Zhao X, B. Zhao, Transformation from nano-ripples to nano-triangle arrays and their orientation control on titanium surfaces by using orthogonally polarized femtosecond laser double-pulse sequences. Appl. Surf. Sci. 588 (2022) 152918. https://doi.org/10.1016/j.apsusc.2022.152918.

[46] Y. Ogata, C. Guo, Nonlinear optics on nano/micro-hierarchical structures on metals: focus on symmetric and plasmonic effects, Nano Rev. Exp. 8 (1) (2017) 1339545, https://doi.org/10.1080/20022727.2017.1339545.

[47] H. Messaoudi, S.K. Das, J. Lange, F. Heinrich, S. Schrader, M. Frohme, R. Grunwald, Femtosecond-Laser Induced Periodic Surface Structures for Surface Enhanced Raman Spectroscopy of Biomolecules, Switzerland:Springer (2015), https://doi.org/10.1007/978-3-319-12217-5_12.

[48] R. Liu, D. Zhang, L. Li, Femtosecond laser induced simultaneous functional nanomaterial synthesis, in situ deposition and hierarchical LIPSS nanostructuring for tunable antireflectance and iridescence applications, J. Mater. Sci. Technol. 89 (2021) 179–185, https://doi.org/10.1016/j.jmst.2021.02.024.

[49] G. Giannuzzi, C. Gaudiuso, R.D. Mundo, L. Mirenghi, F. Fraggelakis, R. Kling, P. M. Lugara, A. Anconab, Short and long term surface chemistry and wetting behaviour of stainless steel with 1D and 2D periodic structures induced by bursts of femtosecond laser pulses, Appl. Surf. Sci. 494 (2019) 1055–1065, https://doi.org/10.1016/j.apsusc.2019.07.126.

[50] T.Y. Hwang, A.V. Vorobyev, C. Guo, Surface-plasmon-enhanced photoelectron emission from nanostructure-covered periodic grooves on metals, Phys. Rev. B 79 (2009), 085425, https://doi.org/10.1103/PhysRevB.79.085425.

[51] A.Y. Vorobyev, V.S. Makin, C. Guo, Brighter light sources from black metal: significant increase in emission efficiency of incandescent light sources, Phys. Rev. Lett. 102 (2009), 234301, https://doi.org/10.1103/PhysRevLett.102.234301.